Aging of lime-based TRM composites under natural environmental conditions

Ali Dalalbashi [1], Bahman Ghiassi[2], Daniel V. Oliveira[3]

ABSTRACT

Textile-reinforced mortar (TRM) composites, composed of textile fibers embedded in an inorganic matrix, have been found to be a sustainable solution for strengthening of an existing masonry or concrete structures. Despite the extensive recent attention in understanding the mechanical performance of these composite, their long-term performance and durability remain unknown. To address this gap, this paper presents a comprehensive experimental and analytical study on the changes in the mechanical response of these composites across scales (from material characterization to bond and tensile tests of TRM composites) under indoor and outdoor conditions. For this purpose, steel and glass fibers with lime-based mortar are used to investigate the pull-out response and the tensile behavior of TRM composites. The results show that the long-term behavior of TRM composites is significantly dependent on the mortar and fiber combination and, therefore, can change notably between different TRMs. It is also observed that lime-based TRMs cannot reach their full mechanical properties under indoor conditions even after 3 years. Outdoor conditions lead to better curing of the samples and achieving significantly higher mechanical properties in these composites. However, it can also lead to a significant deterioration at later ages.

[1] PhD Student, ISISE, University of Minho, Department of Civil Engineering, Azurém, 4800-058 Guimarães, Portugal. E-mail: alidalalbashi@gmail.com
[2] Assistant Professor, Centre for Structural Engineering and Information, Faculty of Engineering, University of Nottingham, Nottingham, United Kingdom. E-mail: bahman.ghiassi@nottingham.ac.uk
[3] Associate Professor, ISISE & IB-S, University of Minho, Department of Civil Engineering, Azurém, 4800-058 Guimarães, Portugal. E-mail: danvco@civil.uminho.pt

Keywords: *TRM/FRCM, Fiber/matrix bond, Tensile behavior, Durability, Aging, Long-term behavior.*

Highlights:

1. *A comprehensive experimental and analytical study on the changes in the mechanical response of TRM composites under indoor and outdoor conditions is conducted.*
2. *136 pull-out and tensile tests are performed on two steel and glass-based TRM composite types.*
3. *TRM mechanical characterizations are investigated for 920 days.*
4. *Ageing effect on the bond behavior of steel-based TRM with two different mortar types is investigated.*

1 Introduction

Textile Reinforced Mortar (TRM) composites, as an externally bonded reinforcement technique, has received extensive attention as a sustainable solution for seismic strengthening of masonry and historical monuments. TRMs, an attractive alternative to the Fiber Reinforced Polymer (FRP) systems, are composed of continuous fabrics embedded in an inorganic matrix [1]. Compared to FRPs, TRMs have some advantages, such as fire resistance and vapor permeability [2,3].

The textile is usually made of glass, steel, basalt, carbon, or natural fibers (e.g., hemp, flax), and matrices are either cementitious or lime-based. Lime mortars are suitable for strengthening masonry and historical monuments because of the compatibility, sustainability issues, breathability, and capability of accommodating structural movements [4–9]. Meanwhile, cementitious matrices are usually used to strengthen strong and new masonry structures [10–13].

TRM composites show a pseudo ductile response and multiple cracking by reaching their maximum bond strength, making them suitable for seismic strengthening applications. This multiple cracking behavior is owed to the fiber-to-mortar bond behavior [14–17]. Understanding this mechanism and its effects on the short-term and long-term performance of these composites is, therefore, of critical importance for having safe and resilient strengthening solutions.

Although the mechanical behavior of lime-based TRMs has been the subject of a large number of recent studies [15,18–23], their long-term performance remains unaddressed and not understood. However, the durability performance of TRM composites has recently received attention from a few studies, in which the effect of freeze-thaw cycles, water attack, alkaline

environment, salt crystallization on the tensile behavior, and TRM-to-substrate bond behavior have been examined [24–29].Aiming at a better understanding of this critical phenomenon, this paper presents, for the first time, a comprehensive experimental and analytical study on the effect of indoor and outdoor aging on the performance of these composites from the material to composite scale.

2 Experiments

The experimental campaign investigates the changes in materials properties (compressive and flexural strength), textile-to-mortar bond behavior, and the tensile response of TRM composites with time under indoor and outdoor environmental conditions. The details of the experimental plan are shown in Table 1. To address this aim, a set of samples (sample details are presented in section 2.1 to 2.4) were placed in the laboratory conditions (20°C, 60 % RH) for 920 days to replicate indoor conditions. Another set was placed outside under direct exposure of rain and sun at the site of the University of Minho to simulate outdoor conditions. The outdoor aged specimens, after initial curing of 90 days in the laboratory, were transported to the outside of the laboratory since January 2017 for 830 days. Fig. 1 shows the changes in mean temperature and humidity of air in the location of samples during the outdoor exposure. A description of the materials, the specimens, and the test setups used are presented in the following section.

2.1 Materials

Materials consisted of two commercially available lime-based mortars as the matrix, referred to M1 and M2 throughout this paper, and the glass and the steel fabrics as reinforcing materials. M1 mortar was a high-ductility hydraulic lime mortar composed of hydraulic lime (NHL), Eco-Pozzolan, natural sand, special additives, synthetic polymers in water dispersion,

and short fibers [30]. M2 mortar was a pure natural NHL 3.5 lime and mineral geobinder base [31]. M1 mortar was prepared by mixing the powder with the liquid provided by the manufacturer (5:1 powder to liquid ratio according to the technical datasheets) in a low-speed mechanical mixer for four minutes to form a homogeneous paste. M2 mortar was prepared by mixing 1 kg powder with 0.212 kg water for seven minutes. According to the technical sheets provided by the manufacturer, the modulus of elasticity of the M1 and M2 mortars were 8 GPa and 9 GPa after 28 days, respectively.

The glass fabric (Fig. 2a) was a woven biaxial fabric mesh made of alkali-resistance fiberglass [32]. Its mesh size and area per unit length were equal to 25 mm×25 mm and 35.27 mm^2/ m, respectively, according to the technical datasheets. The steel fiber (Fig. 2b) was a unidirectional ultra-high tensile steel sheet [33], with a density of 670 g/m^2, an effective area of one cord (five wires) equal to 0.538 mm^2, according to the technical datasheets. Each fiber was made by twisting five individual wires together, three straight filaments wrapped by two filaments at a high twist angle, forming a uniform cord.

These materials were used for the development of the steel-based and the glass-based TRM composite. The fabrics were used with their pair mortar provided by the same manufacturer (glass fibers with M1 mortar and steel fibers with M2 mortar). In addition, to investigate the effect of mortar type on the long-term bond behavior, the steel fiber was used with M1 mortar, too.

2.2 Material characterization tests

The compressive and flexural strength of the mortars was experimentally obtained at different ages (3, 7, 14, 30, 60, 90, 180, and 920 days), according to ASTM C109 [34] and EN 1015-11 [35], respectively. Five cubes (50×50×50 mm^3) and five prismatic (40×40×160 mm^3)

specimens were prepared for each test at each age. Also, fifteen specimens were prepared to study the effect of real environmental exposure on the mechanical properties of the mortars. These specimens were cured in the lab environment for 90 days, stored outside, and then tested at the ages of 180 and 920 days (hence exposed to the real environmental conditions for 90 and 830 days, respectively).

The tests were performed byusing a Lloyd testing machine under load-controlled conditions at a rate of 150 N/s (for compressive tests) and 10 N/s (for flexural tests), as shown in Fig. 3. In the compressive tests, for reducing the friction, a pair of Teflon sheets and oil was placed between the specimen and the compression plates (Fig. 3a). The flexural tests were performed in three-point bending test scheme with a 100 mm distance between the supports (Fig. 3b).

To obtain the tensile strength and elastic modulus of fabrics, a single roving was tested under direct tensile tests. A universal testing machine with a maximum load capacity of 10 kN was used for these tests. The tests were conducted under displacement-controlled conditions at a rate of 0.3 mm/min (Fig. 3c). The free length of the textile for all test specimens was equal to 300 mm. A 100 mm clip gauge located at the center of the specimens and the internal LVDT sensor of the machine measured the fiber deformation along with the tests, as shown in Fig. 3c.

2.3 Pull-out tests

The single-sided pull-out test setup developed and presented in [36] was used for examining the fiber-to-mortar bond performance. The specimens consisted of single fibers embedded in flat disk-shaped mortars with a cross-section of 125×16 mm^2, as shown in Fig. 4a. The free length of the fiber was embedded in an epoxy resin block in 200 mm length and a rectangular cross-sectional area of 10×16 mm^2 [36]. For preparing the pull-out specimens, first, one layer

of mortar with 8 mm thickness was applied inside the wood molds, then fiber was placed on it. Finally, the second layer of mortar with a thickness of 8 mm was applied. The specimens were demolded after 24 hours of preparation and were placed in the lab environmental conditions (20°C, 60 % RH) until testing.

For performing the pull-out tests, a U-shape steel support was used for supporting the specimens to a rigid frame, as shown in Fig. 4a and Fig. 5a. A mechanical clamp was used to grip the top of epoxy resin (thus the fiber) and to perform the tests. Two LVDTs with a 20 mm range and 2-µm sensibility were located at both sides of the epoxy block to record the slip. The averages of these LVDT measurements were presented as the slip in the experimental results. A servo-hydraulic system with a maximum capacity of 25 kN was used. The pull-out test procedure included the application of a constant displacement rate of 1.0 mm/min.

Pull-out tests were performed at 15, 30, 90, 180, 270, and 920 days of mortar age to study the effect of mortar age on the textile-to-mortar bond behavior. The considered embedded lengths were 150 mm and 50 mm for the steel and the glass fibers, respectively. These values were equal to the effective bond length of the samples [37]. Four specimens were prepared and tested for each testing age, resulting in 24 specimens for each the steel-based and the glass-based TRMs. Further, the effect of mortar type on the long-term bond behavior of textile-to-mortar was also examined by comparing the pull-out response of the steel fibers embedded in M1 and M2 mortars at 90 and 920 days of aging.

Twelve samples from each TRM type were also prepared and placed outside the laboratory at the age of 90 days to be exposed to natural environmental conditions. These specimens were tested at the ages of 180, 270, and 920 days. Therefore, specimens were exposed to the natural environmental conditions for 90, 180, and 830 days, respectively

2.4 Tensile tests

Direct tensile tests were conducted on prismatic specimens with a length, width, and thickness of 550 mm, 60 mm, and 10 mm, respectively, as shown in Fig. 4b. The samples consisted of a 100 mm free fiber length at each side and a 350 mm central region in which the fabrics were embedded in the mortar (Fig. 4b). The tensile specimens were prepared as follows: applying the first layer of mortar inside the wood molds (5 mm thickness), placing the fabric mesh, and finally applying the second layer of mortar with 5 mm thickness. The numbers of fibers (parallel to tensile load) in each TRM system were 8 and 3 (with the area ratio of 0.0072 and 0.0044), respectively, for the steel and the glass-based TRM specimens (that was due to specific geometrical properties of each mesh). Finally, samples were covered with plastic for one day, then demolded and cured in the laboratory conditions (20°C, 60% RH) until the test days.

One week before the test date, the free part of fibers was saturated and strengthened with resin to avoid rupture of the fabric in the clamping area. Also, two steel plates ($100\times 75\times 10$ mm^3) were glued to the free part of fibers to apply a uniform load to the fiber mesh.

For performing the tests, a mechanical clamp was used to grip the samples, see Fig. 5b. Two LVDTs with a 20 mm range and 2-μm sensibility placed at both sides of the tensile specimen and recorded the displacement. A servo-hydraulic jack with a maximum capacity of 25 kN applied the direct tensile load to the specimens under a displacement control rate of 0.3 mm/min. The introduced stress was calculated by dividing the load by the cross-section area of the dry textile (steel and glass mesh area were equal to 4.3 mm^2 and 2.65 mm^2, respectively). The strain was measured by dividing the mean value of the displacements recorded from the two LVDTs by their base length (310 mm).

The tensile tests were performed at the mortar ages of 90, 180, 270, and 920 days. Five specimens were tested at each age resulting in 20 specimens for each steel and glass-based TRM type. In addition, 15 specimens from each TRM type were stored in natural environmental conditions and tested at the age of 180, 270, and 920 days (storing outside 90, 180, and 830 days, respectively).

3 Experimental results and discussion

3.1 Material properties

Table 2 and Table 3 summarize the variation of compressive and flexural strength of both mortar types aged under indoor and outdoor conditions. Although the peak compressive strength of both mortars is similar, this value is reached at different ages showing governance of different hydration rates in these two mortars. Also, it can be observed, as opposed to cementitious mortars reaching to the maximum strength after 28 days, the peak compressive and flexural strength is not be reached at a specific age in these lime-based mortars. The peak compressive strength of M1 mortar under indoor conditions is at 60 days (8.3 MPa), while its peak flexural strength only at 180 days (6.0 MPa). Interestingly, a slightly higher compressive strength, but lower flexural strength is obtained under outdoor conditions.

In contrast, the peak compressive strength in M2 mortar (stored indoor) is at 30 days (9.5 MPa), and the peak flexural strength at 920 days (3.1 MPa). In this mortar, under outdoor conditions, both flexural and compressive strength is slightly lower (except for compressive strength at 180 days). Overall, M1 mortar has a higher flexural strength than M2 mortar despite having a lower compressive strength, which indicates a more ductile response of this mortar due to the existence of short fibers in the mortar mix.

It can be indicated that outdoor condition causes both M1 and M2 mortar to reach to higher compressive strength compared to the indoor aged specimens. This observation can be due to the presence of more moisture and more hydration of mortars. In contrast, indoor aged specimens dry faster, and the hydration processes stop.As for the fabrics, direct tensile tests are on single yarns showed average tensile stress, Young's modulus, and rupture strain of 2972 MPa (coefficient of variation: COV= 8 %), 189.3 GPa (COV= 8 %), and 0.0188 mm/mm (COV= 9 %), for the steel cords, as well as 875 MPa (COV= 13 %), 65.9 GPa (COV= 5 %), and 0.0177 mm/mm (COV= 10 %) for the glass yarn.

3.2 Pull-out behavior

For the analysis of the pull-out tests, the main characteristics of the load-slip curves are obtained with age and presented and discussed in sections 3.21 and 3.2.2. These include the peak load, its corresponding slip, initial stiffness, debonding energy, pull-out energy, and chemical bond energy, as reported by [36,38,39]. Debonding energy expresses the energy dissipated during the complete fiber debonding and is measured as the area under the load-slip curve until the peak load [39,40]. The pull-out energy is the energy dissipated by the fiber-to-mortar frictional interface during the dynamic stage. It is measured as the area under the load-slip curve from the peak load until the end [39,41]. Material deformation and new surfaces by cracking characterize the debonding energy [41]. Additionally, the pull-out energy attributes the post-peak behavior of the fiber-to-mortar bond, which is significant in the pseud-ductility behavior of TRM composites. Meanwhile, the chemical bond energy (G_d) is expressed as follows: [42–44]:

$$G_d = \frac{2P_{\Delta}^2}{\pi^2 E_f d_f^3}, \ N/mm \quad \text{..... (1)}$$

In which P_{Δ} is the magnitude of the load drop at the peak load, E_f is the fiber elastic modulus, and d_f is the fiber diameter.

The load-slip curves are also used to extract the bond-slip laws following the stress-based analytical model (shear-lag model) proposed by Naaman et al. [45]. A modified bond-slip law is considered for simulating the slip hardening effect observed in experimental tests, see Fig. 6, [36]. The proposed bond-slip law model is characterized by the bond shear strength ($\tau_{max.}$), the elastic bond modulus (κ), the frictional stress (τ_f), and the slip hardening coefficient (β). In addition, in Fig. 6, d_f and L are the yarn diameter and bond length, respectively. η reflects the changes in the slope of the pull-out curve and υ is the rigid body displacement of the yarn after full debonding. The bond-slip laws parameters are obtained with the aim of the analytical model, and its accuracy is evaluated by predicting the pull-out curves as followed. The analytical pull-out modeling consists of two primary and secondary problems [45]. The output of the primary problem is the bond-slip law parameters ($\tau_{max.}$, τ_f, and κ). In the secondary problem, the load-slip curve is predicted from the obtained bond-slip law. For more details of how to calibrate the bond-slip laws parameter and the modeled pull-out response, the reader is referred to [36].

3.2.1 Steel-based TRM

The failure mode for all the specimens is fiber slipping/pull-out from the mortar. The pull-out curves at all ages show the typical linear, nonlinear, and dynamic stages with a drop of the load after the peak load (see, for example, the results obtained from samples tested at 15 days in Fig. 7a). This sudden drop load shows the transition from chemical/frictional bond to frictional bond and indicates that the frictional bond is smaller than the adhesive bond in this system [39,42,44,46,47]. After this load drop, a slip hardening behavior (forming a second

peak load) and then a softening response until the end of the tests is observed [39,44,47–50]. Comparing the load-slip curves of the samples tested at different ages under indoor conditions, Fig. 7b, shows that in general, the bond behavior is improved with time even until 920 days, a slight decrement of bond performance is also observed at some ages. This behavior is because of the increase in the M2 mortar strength.

The role of the mortar type seems to be significant for the bond performance of indoor aged samples, as shown in Fig. 7c. Specimens prepared with M1 mortar show a better bond performance at 90 days but a worse one at 920 days than specimens prepared with M2 mortar. It seems that although pull-out samples prepared with M1 mortar gain higher strengths in early ages, bond deterioration or mortar shrinkage in longer ages governs their performance at later ages. Also, a comparison between the pull-out response of M1 mortar at 90 and 920 days shows (Fig. 7c) that the transition from the progressive debonding stage to the dynamic stage has changed from a smooth and upward trend to a sudden drop in the pull-out load.

Comparing the pull-out curves of indoor and outdoor aged samples (made of M2 mortar), Fig. 7d, shows that generally, outdoor aged samples have a better bond performance. This observation can be due to a higher hydration degree achieved in the samples aged under outdoor conditions. Clearly, hydraulic lime-based mortars aged under indoor conditions have a considerably slower hydration degree and thus the bond performance. The peak load of samples aged (at 920 days) under outdoor conditions is 1125.9 N, which is 1.19 times that of samples aged under indoor conditions. It should also be noted that samples aged under outdoor conditions reached a peak load of 1550.3 N at 270 days showing a deterioration mechanism afterward until 920 days.

To better understand the role of environmental conditions, the changes in the key characteristics of the pull-out curves with time is presented in Fig. 8. Here, the individual sample results are all presented together with a nonlinear regression line showing the general trend of the results with time. The mean values of pull-out parameters of indoor and outdoor specimens are presented in Table A1 and Table A2 in the appendix section. It can be observed that the peak load, the initial stiffness, the deboning energy, the chemical bond energy, and the pull-out energy show, in general, an incremental trend up until 270 days, and then the values have decreased until the end of the tests in outdoor aged samples. Meanwhile, in indoor aged samples, these properties reached their peak value at an early age and, after that, do not show a significant change with time except for the chemical bond energy and initial stiffness, which are slightly decreased in the initial stage of exposure. As expected, the variation of the experimental results is also higher in the samples aged under outdoor conditions.

The average bond-slip laws are also presented in Fig. 9. Again, the bond strength, $\tau_{max.}$, (Fig. 9a), and the frictional strength, τ_f, (Fig. 9b) show an incremental trend in outdoor aged samples (bond strength decreases from 270 days to 920 days), while no significant changes can be observed in indoor aged samples. The bond modulus (κ), however, seems to be increasing significantly in outdoor aged samples, but slightly decreasing in the early ages in indoor aged samples (note a high variation is observed in the results for this parameter), Fig. 9c. At the same time, the slip hardening coefficient (β) shows an increasing trend for both indoor and outdoor aged samples (Fig. 9d); nevertheless, the indoor aged specimens show higher values in contrast to the outdoor aged specimens. A comparison between τ_f and β shows the higher frictional stress, the lower slip hardening coefficient. The mean values of the bond-slip laws

for indoor and outdoor specimens are also presented in Table A3 and Table A4 for interested readers.

3.2.2 Glass-based TRM

The pull-out curves of the individual samples, the experimental average, and the analytical curves of the glass-based TRM are presented in Fig. 10. These specimens, in contrast to steel-based TRMs, do not show a sudden load drop after the peak load; thus, the transition from the progressive debonding to the dynamic stage is smooth. This behavior can be due to the insufficient curing condition of the M1 mortar, followed by the weak bond at the fiber-to-mortar interface. Comparing the pull-out curves tested at different ages and under indoor conditions (Fig. 10b) shows that at early and late ages (until 30 days and after 270 days), the slip hardening is followed by a softening in the pull-out curves. However, at 90 and 180 days, the slip hardening is followed by a second slip hardening effect leading to significant absorption of energy. This change of final slip softening at early ages to slip hardening seems to be a result of further hydration of the mortar. Nevertheless, at later ages, it seems that a sort of bond deterioration or mortar shrinkage by forming micro-cracks at the bond interface has occurred, which led to a slip softening behavior.

Comparison of the indoor and outdoor aged samples indicates again that generally, outdoor aged samples show a better bond performance compared to indoor aged samples, see Fig. 10c. This behavior is in line with what is observed for the M1 mortar changes at indoor and outdoor conditions. As also observed in indoor aged samples, a degradation of the bond performance can also be observed in the samples aged under outdoor conditions at later ages.

The key characteristics of the pull-out response, when compared in Fig. 11, show that the peak load and debonding energy of outdoor samples are slightly higher than the corresponding

specimens tested in the indoor condition.However, both the peak load and debonding energy show a decline behavior from 270 days to 920 days in outdoor aged samples. The initial stiffness of the outdoor aged samples is significantly higher than the indoor aged samples becoming more than three times at 920 days, owing to better curing conditions or higher hydration of the M1 mortar. Moreover, both the debonding energy and the pull-out energy show an increase trend for indoor aged samples, energy desorption is always smaller than that of outdoor aged samples up until the end of the tests where they become close. Increasing the energy desorption at the early ages of outdoor exposure can be due to improving the bond of fiber-to-mortar. By increasing the exposure ages, the bond declined due to deterioration, shrinkage, or micro-cracks. Again, the experimental mean values are presented in Table A5 and Table A6.

The changes in the bond-slip law parameters are shown in Fig. 12, Table A7, and Table A8. The bond strength, $\tau_{max.}$, is always higher in outdoor aged samples than indoor samples (almost twice at 920 days), as shown in Fig. 12a. On the other hand, the frictional stress, τ_f, shows an incremental trend (initially with higher rates and then lower rates) in samples under indoor conditions, in contrast to the outdoor aged samples in which a significant deterioration can be observed from 270 to 920 days. By contrast, the bond modulus, κ, and slip hardening coefficient, β, do not show a significant change in indoor aged samples but increase significantly with time in outdoor aged samples. These observations can show the effect of higher hydration of the M1 mortar on the parameters of the bond-slip law

3.3 Tensile behavior

Fig. 13 shows the schematic tensile behavior of TRM composites [1,18,19,21,51–53], in which the tensile load was applied to TRM composites. While in this study, the load is applied

directly to the fiber meshes. Three stages are usually identified in the tensile response: (stage I) a linear stage which presents the behavior of uncracked composite material [51–53]; (stage II) a crack development stage in which multiple cracks are formed in the specimens. The distance, the width, and the number of cracks are strictly dependent on the fiber-to-mortar bond behavior in this stage [51–53]. Finally, (stage III), no further cracking occurs, and the load is only resisted by the bundles/yarns. The peak tensile stress (σ), the strain corresponding to the peak stress (ε) and tensile modulus (E) in each stage, and the saturated crack spacing are the key characteristics of the tensile response of these composites and therefore will be discussed in the next sections for each aging condition and TRM type.

3.3.1 Steel-based TRM

The typical tensile stress-strain response of individual steel-based TRMs at 90 days, together with their experimental average curves, are presented in Fig. 14a. In all the specimens, fiber rupture was the governing failure mode. In addition to the three typical stages of the tensile response, explained previously, a final softening stage can be observed in the stress-strain curves. This final softening is probably due to the non-uniform distribution of the stresses among the cords or the step-by-step failure of wires. Cracking of the mortar can be clearly observed in the samples Fig. 14b. Many cracks have formed, showing the balance between the bond and mortar strength and suitable textile-to-mortar bond behavior in these samples.

At first glance, no significant change is observed in the tensile response of samples aged under indoor conditions, Fig. 14c, or the samples aged under outdoor conditions (despite the final tension strength), Fig. 14d, with time. However, looking at the changes in the main characteristics of the tensile response, Fig. 15, shows interesting trends. Only a slight increase can be observed in the first cracking stress, σ_1, with time in indoor aged samples. However,

the cracking strength is increased until 270 days and then decreased until the end of the tests in the outdoor aged samples. At all times, however, outdoor samples show higher cracking stress than the indoor samples, which can be again attributed to a higher hydration degree of the mortar. These observations are in line with the observed changes in the mechanical properties of the mortars reported in previous sections. The stress corresponding to the end of stage II, σ_2, increases notably with time in both indoor and outdoor aged samples. Again, outdoor aged samples show a higher σ_2 than indoor aged samples. In contrast, σ_3, shows an initial decrease and then an increase in both cases. As for stiffness, E_1 is increased initially and then decreased, E_2, increases, and E_3 does not show any significant changes with time. The saturation crack spacing of the samples gradually decreases over time, Fig. 16a. The mean values are also explicitly presented in Table A9 and Table A10.

3.3.2 Glass-based TRM

The typical tensile stress-strain response of individual glass-based TRMs (at 90 days), together with their experimental average curves, are presented in Fig. 17a. In all the specimens, again, fiber rupture was the governing failure mode. Although the three stages of the tensile response are identified in the curves, no fluctuation in the crack developing stage can be observed, which is due to the small number of cracks formed in these samples and/ or the low tensile strength of the glass fibers (Fig. 17b).

No significant change is observed in the tensile response of samples aged under indoor conditions, Fig. 17c, though the samples aged under outdoor conditions, show the tensile behavior declines by increasing the exposure, as presented in Fig. 17d. However, an in-depth look at the changes in the main characteristics of the tensile response (Fig. 18) shows some differences between the samples aged under indoor and outdoor conditions. As opposed to

steel-based TRM, the first cracking stress, σ_1, decreases with time. This decrease is significantly higher in outdoor aged specimens in the first 270 days, which is then recovered to some extent until the end of the tests. The stress corresponding to the end of stage II, σ_2, increases with time in indoor aged samples but decreases in outdoor aged samples. σ_3, shows a slight decrease in indoor aged samples and a significant one in outdoor aged samples. This observation shows the sensitivity of the glass yarns to outdoor environmental conditions, which has led to their mechanical degradation. As for stiffness, E_1 increases with time for indoor aged samples and decreases for outdoor aged samples, E_2 increases in indoor aged samples but shows a decrease after 270 days in outdoor aged samples and E_3 decreases in both cases. In contrast to Steel-based TRM, the crack spacing is decreased in indoor aged but decreases in outdoor aged samples, Fig. 16b. The mean values are also explicitly presented in Table A11 and Table A12.

4 Conclusions

The effect of indoor and outdoor aging on the micro- and macro-mechanical behavior of two lime-based TRMs were examined in this paper. A comprehensive experimental and analytical study was performed to investigate the changes of the mortar mechanical properties, the textile-to-mortar bond behavior, and the TRM tensile response was characterized until 920 days of aging. From the results obtained in this study, the following conclusions can be drawn:

- In lime-based TRMs, special attention needs to be given to the hydration degree of the mortar and its effects on the short-term and long-term performance of those composites. 30 days curing age testing, as usually used for cementitious matrices, does not seem to be particularly a good reference for hydraulic lime-based TRMs. With the large variety of the characteristics of the existing lime-based mortars, it is also difficult

to propose a specific time that is representative of the long-term behavior of those composites. The experimental results showed a good correlation between the changes in the textile-to-mortar bond behavior and the flexural strength of the mortar. Flexural strength is, therefore, proposed to be used as an indication for evaluating the changes in the response of lime-based TRMs in the lack of more detailed results.

- As expected, the mortar type was found to have a significant influence on the short-term and long-term bond performance and therefore cracking behavior of TRMs.
- In both systems studied here, TRMs did not reach their highest performance under indoor conditions even after 920 days. This means that under indoor conditions the hydration of the mortar is still in progress. This was more noticeable in the steel-based TRM, which showed a much lower bond strength when cured under indoor conditions than outdoor conditions. Advanced curing conditions may be useful for accelerating hydration such as autoclave, steam, and strength achievement. Outdoor conditions in both systems lead to better mechanical performance in both systems and led to the deterioration in the long-term. The degree of this deterioration, which was significant in some cases) was observed to be dependent on the TRM type (fiber-mortar combination).
- The difference between the tensile response and cracking behavior of the TRM composites under indoor and outdoor conditions was also noticeable and was observed to be dependent on the TRM type. In the steel-based TRM, aging led to the decrement of the crack spacing and no specific change in the final tensile strength. Meanwhile, in the glass-based TRM, the effect of outdoor exposure was significant in terms of crack spacing (increased) and tensile strength (decreased).

- Due to the high humidity and rain, the hydration rate of the hydraulic lime-based mortars was high, which increased the strength of the specimens. In contrast, owing to the constant humidity inside the laboratory, the mortars showed low hydration rates, and their strength gradually increased over 920 days.

5 Acknowledgments

This work was partly financed by FEDER funds through the Competitivity Factors Operational Program (COMPETE) and by national funds through the Foundation for Science and Technology (FCT) within the scope of the project POCI-01-0145-FEDER-007633. The support to the first author through grant SFRH/BD/131282/2017 is acknowledged. Besides, the authors would like to thank the Kerakoll Company for supplying the GeoCalce Fino mortar as well as GeoSteel G600 fibers.

6 References

[1] B. Ghiassi, D. V Oliveira, V. Marques, E. Soares, H. Maljaee, Multi-level characterization of steel reinforced mortars for strengthening of masonry structures, Mater. Des. 110 (2016) 903–913. https://doi.org/10.1016/j.matdes.2016.08.034.

[2] S.M. Raoof, L.N. Koutas, D.A. Bournas, Textile-reinforced mortar (TRM) versus fibre-reinforced polymers (FRP) in flexural strengthening of RC beams, Constr. Build. Mater. 151 (2017) 279–291. https://doi.org/10.1016/j.conbuildmat.2017.05.023.

[3] M.R. Valluzzi, V. Modena, Claudio, G. de Felice, Current practice and open issues in strengthening historical buildings with composites, Mater. Struct. 47 (2014) 1971–1985. https://doi.org/10.1617/s11527-014-0359-7.

[4] S. Barr, W.J. McCarter, B. Suryanto, Bond-strength performance of hydraulic lime and natural cement mortared sandstone masonry, Constr. Build. Mater. 84 (2015) 128–135. https://doi.org/10.1016/j.conbuildmat.2015.03.016.

[5] V. Pavlík, M. Uzáková, Effect of curing conditions on the properties of lime, lime–metakaolin and lime–zeolite mortars, Constr. Build. Mater. 102 (2016) 14–25. https://doi.org/10.1016/j.conbuildmat.2015.10.128.

[6] J. Lanas, J.L. Perez Bernal, M.A. Bello, J.I. Alvarez, Mechanical properties of masonry repair dolomitic lime-based mortars, Cem. Concr. Res. 36 (2006) 951–960. https://doi.org/10.1016/j.cemconres.2005.10.004.

[7] C. Groot, RILEM TC 203-RHM: Performance requirements for renders and plasters, Mater. Struct. 45 (2012) 1277–1285. https://doi.org/10.1617/s11527-012-9916-0.

[8] J. Lanas, J.I. Alvarez, Masonry repair lime-based mortars: Factors affecting the mechanical behavior, Cem. Concr. Res. 33 (2003) 1867–1876. https://doi.org/10.1016/S0008-8846(03)00210-2.
[9] R.M.H. Lawrence, T.J. Mays, P. Walker, D.D. Ayala, Determination of carbonation profiles in non-hydraulic lime mortars using thermogravimetric analysis, Thermochim. Acta. 444 (2006) 179–189. https://doi.org/10.1016/j.tca.2006.03.002.
[10] S. Yin, L. Jing, M. Yin, B. Wang, Mechanical properties of textile reinforced concrete under chloride wet-dry and freeze-thaw cycle environments, Cem. Concr. Compos. 96 (2019) 118–127. https://doi.org/10.1016/j.cemconcomp.2018.11.020.
[11] A. Caggiano, H. Xargay, P. Folino, E. Martinelli, Experimental and numerical characterization of the bond behavior of steel fibers recovered from waste tires embedded in cementitious matrices, Cem. Concr. Compos. (2015). https://doi.org/10.1016/j.cemconcomp.2015.04.015.
[12] C. Caggegi, F.G. Carozzi, S. De Santis, F. Fabbrocino, F. Focacci, Ł. Hojdys, E. Lanoye, L. Zuccarino, Experimental analysis on tensile and bond properties of PBO and aramid fabric reinforced cementitious matrix for strengthening masonry structures, Compos. Part B Eng. 127 (2017). https://doi.org/10.1016/j.compositesb.2017.05.048.
[13] T. D'Antino, L.H. Sneed, C. Carloni, C. Pellegrino, Influence of the substrate characteristics on the bond behavior of PBO FRCM-concrete joints, Constr. Build. Mater. 101 (2015). https://doi.org/10.1016/j.conbuildmat.2015.10.045.
[14] U. Häußler-Combe, J. Hartig, Bond and failure mechanisms of textile reinforced concrete (TRC) under uniaxial tensile loading, Cem. Concr. Compos. 29 (2007) 279–289. https://doi.org/10.1016/j.cemconcomp.2006.12.012.
[15] G.P. Lignola, C. Caggegi, F. Ceroni, S. De Santis, P. Krajewski, P.B. Lourenço, M. Morganti, C. (Corina) Papanicolaou, C. Pellegrino, A. Prota, L. Zuccarino, Performance assessment of basalt FRCM for retrofit applications on masonry, Compos. Part B Eng. 128 (2017) 1–18. https://doi.org/10.1016/j.compositesb.2017.05.003.
[16] R. Barhum, V. Mechtcherine, Effect of short, dispersed glass and carbon fibres on the behaviour of textile-reinforced concrete under tensile loading, Eng. Fract. Mech. 92 (2012) 56–71. https://doi.org/10.1016/j.engfracmech.2012.06.001.
[17] W. Brameshuber, ed., RILEM TC 201-TRC: Textile reinforced concrete- state-of-the-art, RILEM, Bagneux, 2006.
[18] S. De Santis, F. Ceroni, G. de Felice, M. Fagone, B. Ghiassi, A. Kwiecień, G.P. Lignola, M. Morganti, M. Santandrea, M.R. Valluzzi, A. Viskovic, Round Robin Test on tensile and bond behaviour of Steel Reinforced Grout systems, Compos. Part B Eng. 127 (2017) 100–120. https://doi.org/10.1016/j.compositesb.2017.03.052.
[19] S. De Santis, G. de Felice, Tensile behaviour of mortar-based composites for externally bonded reinforcement systems, Compos. PART B. 68 (2015) 401–413. https://doi.org/10.1016/j.compositesb.2014.09.011.
[20] M. Leone, M.A. Aiello, A. Balsamo, F.G. Carozzi, F. Ceroni, M. Corradi, M. Gams, E. Garbin, N. Gattesco, P. Krajewski, C. Mazzotti, D. Oliveira, C. Papanicolaou, G. Ranocchiai, F. Roscini, D. Saenger, Glass fabric reinforced cementitious matrix: Tensile properties and bond performance on masonry substrate, Compos. Part B Eng. 127 (2017). https://doi.org/10.1016/j.compositesb.2017.06.028.
[21] T. D'Antino, C. Papanicolaou, Mechanical characterization of textile reinforced

inorganic-matrix composites, Compos. Part B Eng. 127 (2017). https://doi.org/10.1016/j.compositesb.2017.02.034.
[22] A. Bilotta, F. Ceroni, E. Nigro, M. Pecce, Experimental tests on FRCM strengthening systems for tuff masonry elements, Constr. Build. Mater. 138 (2017) 114–133. https://doi.org/10.1016/j.conbuildmat.2017.01.124.
[23] F.G. Carozzi, C. Poggi, Mechanical properties and debonding strength of Fabric Reinforced Cementitious Matrix (FRCM) systems for masonry strengthening, Compos. Part B Eng. 70 (2015) 215–230. https://doi.org/10.1016/j.compositesb.2014.10.056.
[24] K. Al-Lami, T. D'Antino, P. Colombi, Durability of fabric-reinforced cementitious matrix (FRCM) composites: A review, Appl. Sci. 10 (2020). https://doi.org/10.3390/app10051714.
[25] B. Ghiassi, Mechanics and durability of textile reinforced mortars: a review of recent advances and open issues, RILEM Tech. Lett. 4 (2019) 130–137. https://doi.org/10.21809/rilemtechlett.2019.99.
[26] I.G. Colombo, M. Colombo, M. Prisco, Tensile behavior of textile reinforced concrete subjected to freezing-thawing cycles in un-cracked and cracked regimes, Cem. Concr. Res. 73 (2015) 169–183. https://doi.org/10.1016/j.cemconres.2015.03.001.
[27] E. Franzoni, C. Gentilini, M. Santandrea, S. Zanotto, C. Carloni, Durability of steel FRCM-masonry joints: effect of water and salt crystallization, Mater. Struct. 50 (2017) 1–16. https://doi.org/10.1617/s11527-017-1070-2.
[28] J. Donnini, Durability of glass FRCM systems: Effects of different environments on mechanical properties, Compos. Part B. (2019) 107047. https://doi.org/10.1016/j.compositesb.2019.107047.
[29] E. Franzoni, M. Santandrea, C. Gentilini, A. Fregni, C. Carloni, The role of mortar matrix in the bond behavior and salt crystallization resistance of FRCM applied to masonry, Constr. Build. Mater. 209 (2019) 592–605. https://doi.org/10.1016/j.conbuildmat.2019.03.059.
[30] Planitop HDM Restauro- 1071-2-2012, MAPEI. (2012). https://www.mapei.com/it/en/products-and-solutions/products/detail/planitop-hdm.
[31] GeoCalce Fino, Kerakoll. (2016). https://shop.vittoriosabato.it/uploads/products/attachments/561_KERAKOLL BIOCALCE FINO KG25.pdf.
[32] Mapegride G220- 1033-7-2019 (GB), MAPEI. (2019). https://www.mapei.com/it/en/products-and-solutions/products/detail/mapegrid-g-220.
[33] GeoSteel G600 Code: E865 2014/07, Kerakoll. (2014). https://products.kerakoll.com/en/p/geosteel-g600.
[34] ASTM C109/C109M-05, Standard test method for compressive strength of hydraulic cement mortars (Using 2-in. or [50-mm] Cube Specimens), 2005. https://doi.org/10.1520/C0109_C0109M-05.
[35] BS EN 1015-11, Methods of test for mortar for masonry. Determination of flexural and compressive strength of hardened mortar, 1999.
[36] A. Dalalbashi, B. Ghiassi, D.V. Oliveira, A. Freitas, Effect of test setup on the fiber-to-mortar pull-out response in TRM composites: experimental and analytical modeling, Compos. Part B Eng. 143 (2018) 250–268. https://doi.org/10.1016/j.compositesb.2018.02.010.

[37] A. Dalalbashi, B. Ghiassi, D.V. Oliveira, A. Freitas, Fiber-to-mortar bond behavior in TRM composites: effect of embedded length and fiber configuration, Compos. Part B Eng. 152 (2018) 43–57. https://doi.org/10.1016/j.compositesb.2018.06.014.
[38] B. Mobasher, Mechanics of Fiber and Textile Reinforced Cement Composites, Taylor & Francis Group, London- New York, 2012.
[39] D.L. Naik, A. Sharma, R.R. Chada, R. Kiran, T. Sirotiak, Modified pullout test for indirect characterization of natural fiber and cementitious matrix interface properties, Constr. Build. Mater. 208 (2019) 381–393. https://doi.org/10.1016/j.conbuildmat.2019.03.021.
[40] S.Y. Zhang, Debonding and cracking energy release rate of the fiber/matrix interface, Compos. Sci. Technol. 58 (1998) 331–335. https://doi.org/10.1016/S0266-3538(97)00073-0.
[41] J.M. Alwan, A. Naaman, W. Hansen, Pull-Out work of steel fibers from cementitious composites : analytical investigation, Cem. Concr. Compos. 13 (1991) 247–255. https://doi.org/10.1016/0958-9465(91)90030-L.
[42] W.P. Boshoff, V. Mechtcherine, G.P.A.G. van Zijl, Characterising the time-dependant behaviour on the single fibre level of SHCC: Part 2: The rate effects on fibre pull-out tests, Cem. Concr. Res. 39 (2009) 787–797. https://doi.org/10.1016/j.cemconres.2009.06.006.
[43] T. Kanda, V.C. Li, Interface property and apparent strength of a high strength hydrophilic fiber in cement matrix, J. Mater. Civ. Eng. 10 (1998) 5–13. https://doi.org/10.1061/(ASCE)0899-1561(1998)10:1(5).
[44] Z. Lin, T. Kanda, V.C. Li, On interface property characterization and performance of fiber reinforced cementitious composites, J. Concr. Sci. Eng. RILEM. 1 (1999) 173–184. http://hdl.handle.net/2027.42/84718.
[45] A.E. Naaman, G.G. Namur, J.M. Alwan, H.S. Najm, Fiber pullout and bond slip. i: analytical study, J. Struct. Eng. 117 (1991) 2769–2790. https://doi.org/10.1061/(ASCE)0733-9445(1991)117:9(2769).
[46] V.C. Li, H.C. Wu, Y.W. Chan, Interfacial property tailoring for pseudo strain-hardening cementitious composites, Adv. Technol. Des. Fabr. Compos. Mater. Struct. Eng. Appl. Fract. Mech. 14 (1995) 261–268. https://doi.org/10.1007/978-94-015-8563-7_18.
[47] C. Redon, V.C. Li, C. Wu, H. Hoshiro, T. Saito, A. Ogawa, Measuring and modifying interface properties of PVA fibers in ECC matrix, J. Mater. Civ. Eng. 13 (2001) 399–406. https://doi.org/10.1061/(ASCE)0899-1561(2001)13:6(399).
[48] Z. Lin, V.C. Li, Crack bridging in fiber reinforced cementitious composites with slip-hardening interfaces, J. Mech. Phys. Solids. 45 (1997) 763–787. https://doi.org/10.1016/S0022-5096(96)00095-6.
[49] E.A. Schauffert, G. Cusatis, D. Pelessone, J.L. O'Daniel, J.T. Baylot, Lattice discrete particle model for fiber-reinforced concrete. II: Tensile fracture and multiaxial loading behavior, J. Eng. Mech. 138 (2011) 834–841. https://doi.org/10.1061/(asce)em.1943-7889.0000392.
[50] K.H. Tsai, K.S. Kim, The micromechanics of fiber pull-out, J. Mech. Phys. Solids. 44 (1996) 1147–1159. https://doi.org/10.1016/0022-5096(96)00019-1.
[51] P. Larrinaga, C. Chastre, H.C. Biscaia, J.T. San-José, Experimental and numerical

modeling of basalt textile reinforced mortar behavior under uniaxial tensile stress, Mater. Des. 55 (2014) 66–74. https://doi.org/10.1016/j.matdes.2013.09.050.
[52] I.G. Colombo, A. Magri, Z. Giulio, M. Colombo, M. di Prisco, Textile Reinforced Concrete : experimental investigation on design parameters, Mater. Struct. (2013). https://doi.org/10.1617/s11527-013-0017-5.
[53] L. Mercedes, L. Gil, E. Bernat-Maso, Mechanical performance of vegetal fabric reinforced cementitious matrix (FRCM) composites, Constr. Build. Mater. 175 (2018) 161–173. https://doi.org/10.1016/j.conbuildmat.2018.04.171.

List of Figures

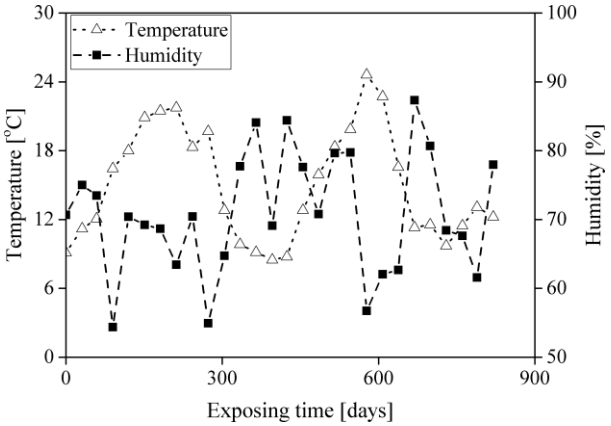

Fig. 1. Changes of the temperature and humidity of air at Guimarães region during outdoor exposure conditions.

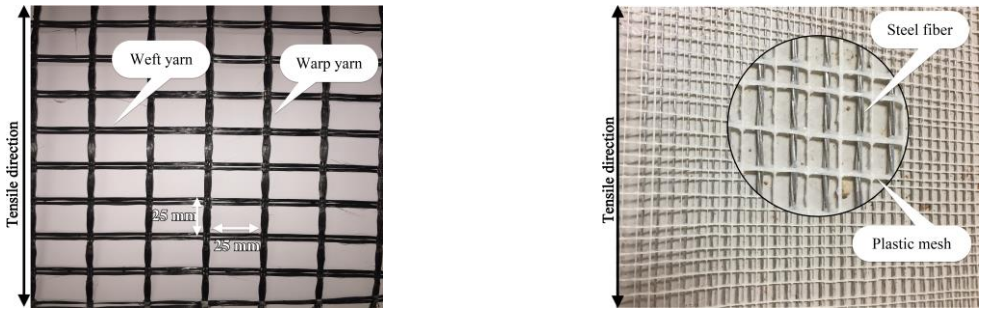

(a) (b)

Fig. 2. Fiber configuration: (a) glass mesh; (b) steel mesh.

(a) (b) (c)

Fig. 3. Mechanical characterization tests: (a) compressive mortar test; (b) flexural mortar test; (c) fiber direct tensile test.

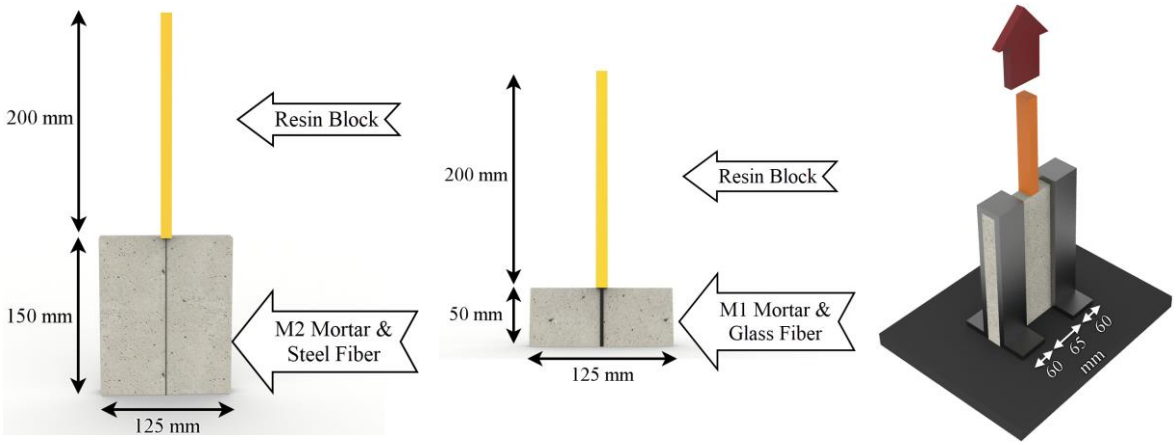

(a)

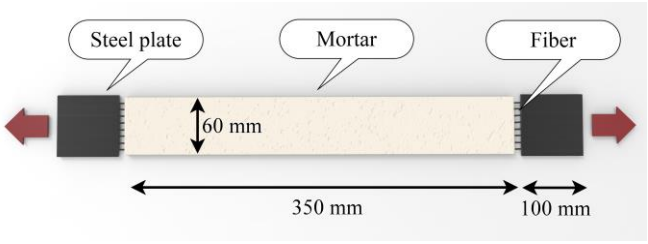

(b)

Fig. 4. Specimens' configurations and corresponding test setups: (a) pull-out test; (b) tensile test.

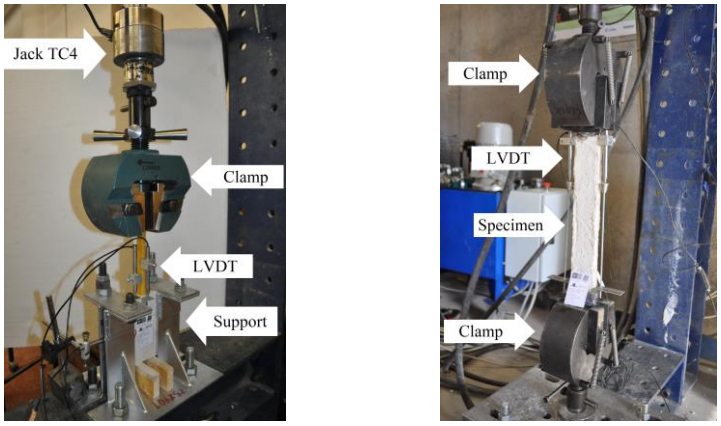

(a) (b)

Fig. 5. Test setups and instrumentation used: (a) pull-out test; (b) tensile test.

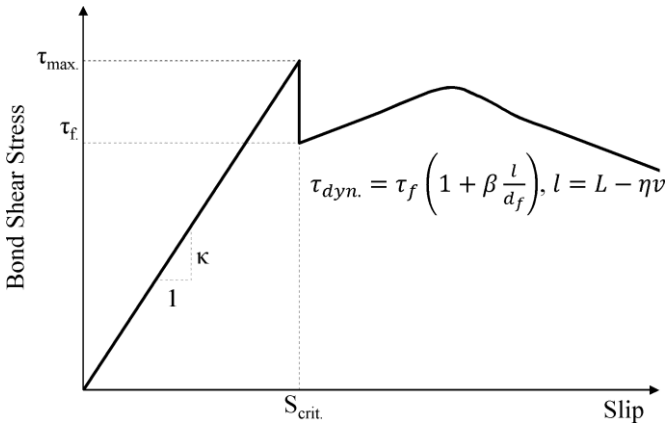

Fig. 6. Bond shear stress-slip law.

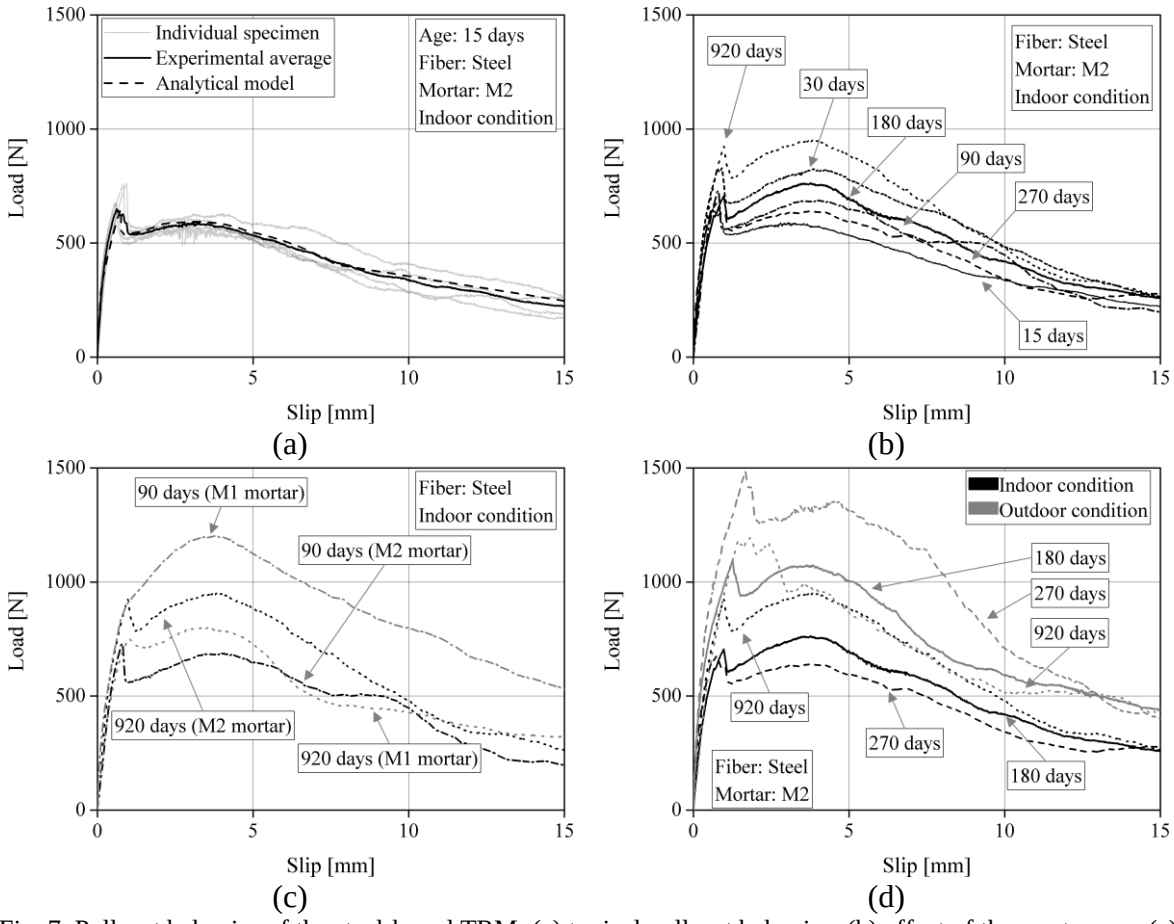

Fig. 7. Pull-out behavior of the steel-based TRM: (a) typical pull-out behavior; (b) effect of the mortar age; (c) effect of the mortar type; (d) effect of environmental condition.

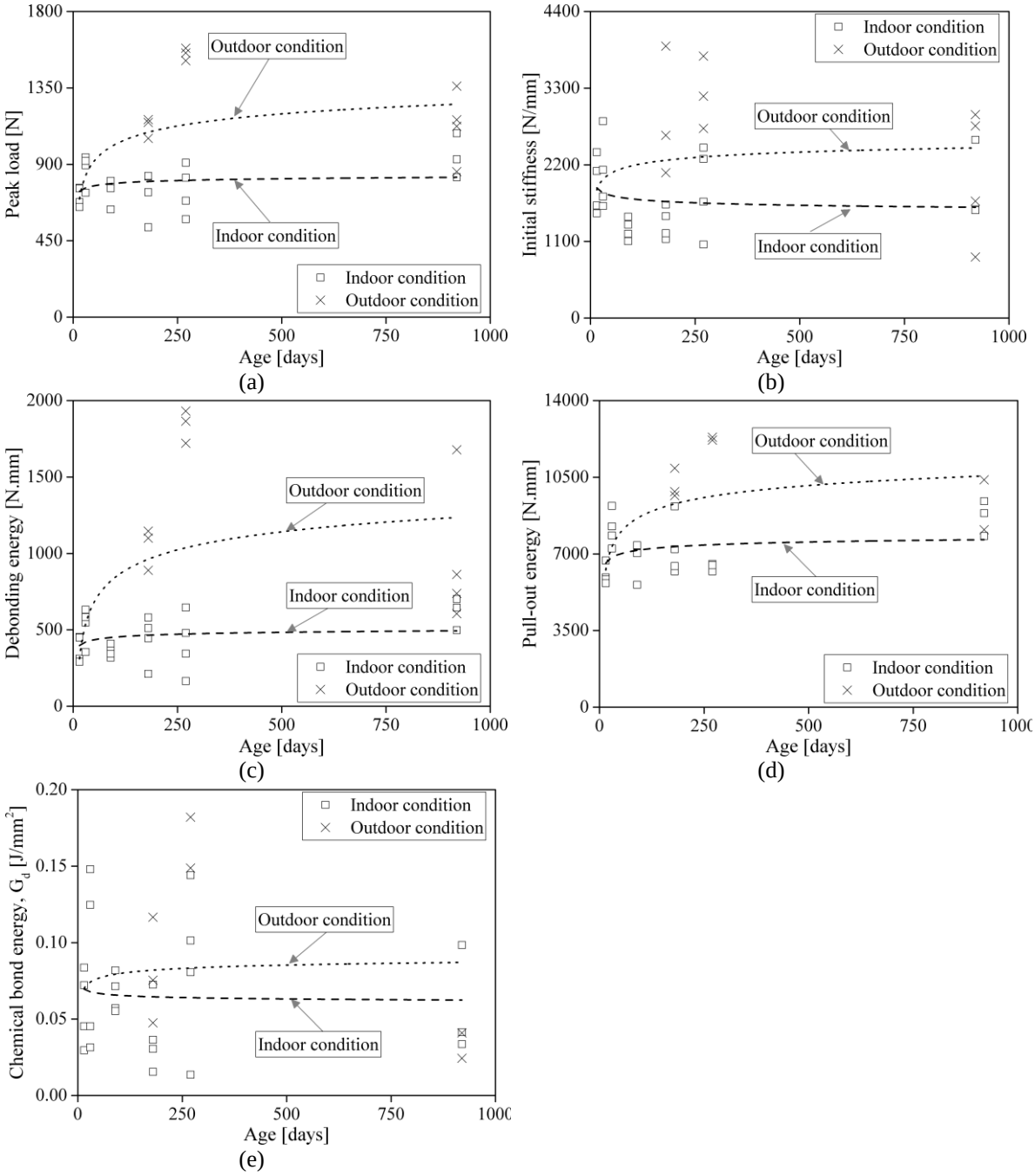

Fig. 8. Pull-out behavior parameters of the steel-based TRM: (a) peak load; (b) initial stiffness; (c) debonding energy; (d) pull-out energy; (e) chemical bond energy.

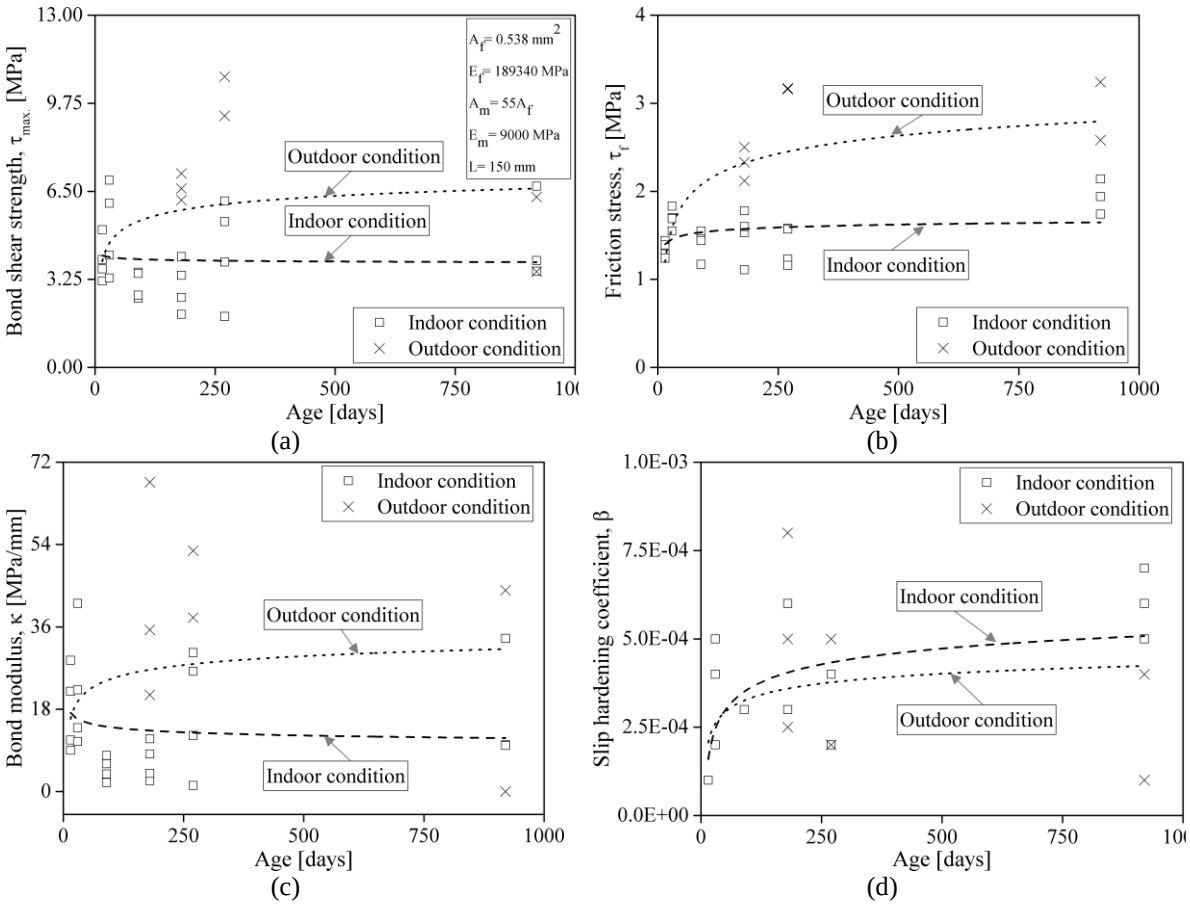

Fig. 9. Bond-slip law parameters of the steel-based TRM: (a) bond shear strength; (b) friction stress; (c) bond modulus; (d) slip hardening coefficient.

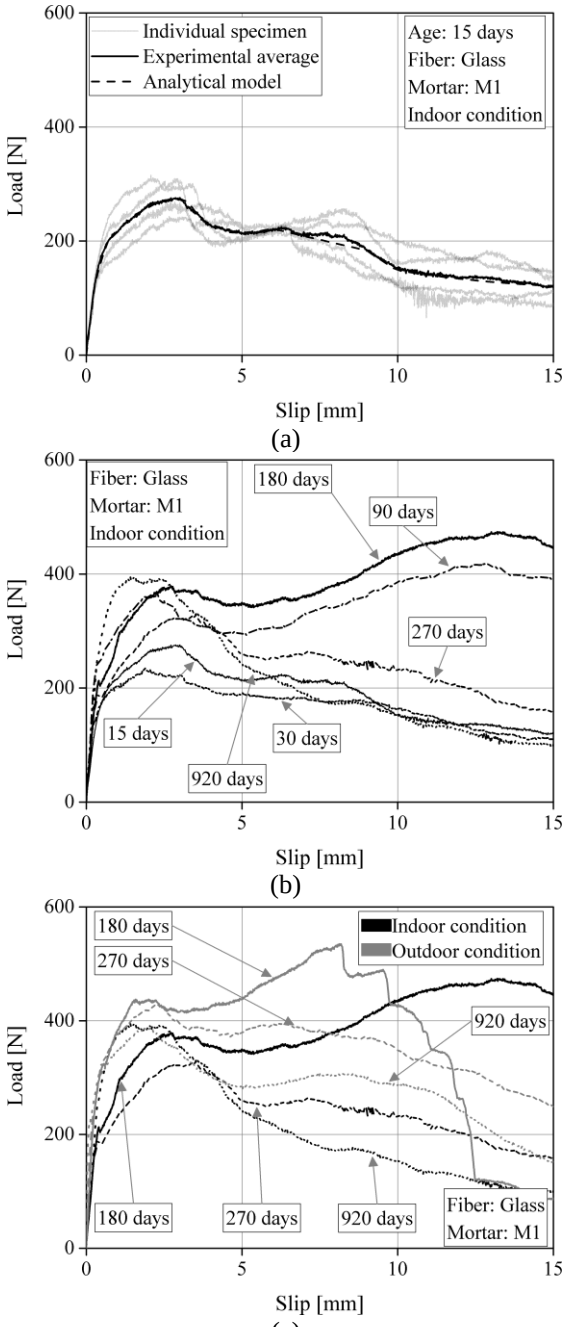

Fig. 10. Pull-out behavior of the glass-based TRM: (a) typical pull-out behavior; (b) effect of the mortar age; (c) effect of environmental conditions.

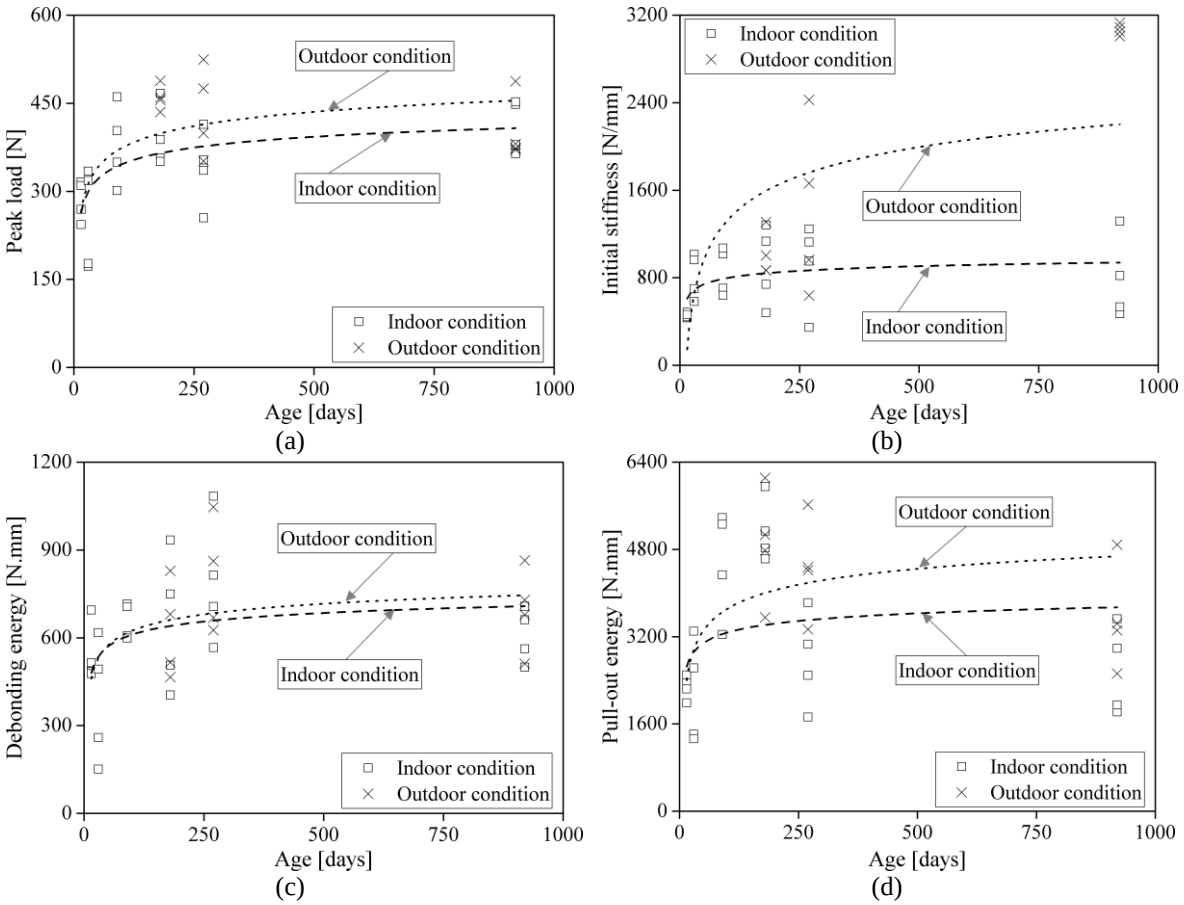

Fig. 11. Pull-out behavior parameters of the glass-based TRM: (a) peak load; (b) initial stiffness; (c) debonding energy; (d) pull-out energy.

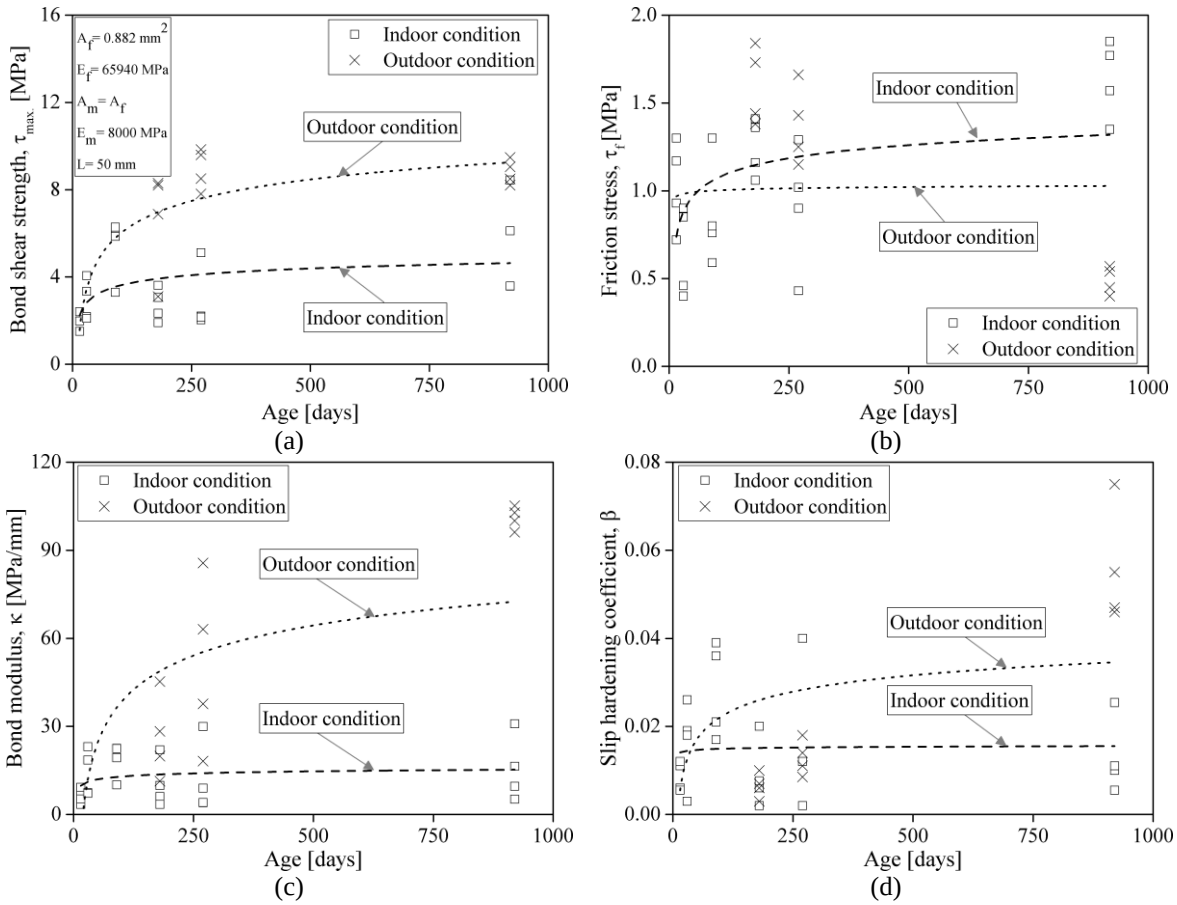

Fig. 12. Bond-slip law parameters of the glass-based TRM: (a) bond shear strength; (b) friction stress; (c) bond modulus; (d) slip hardening coefficient.

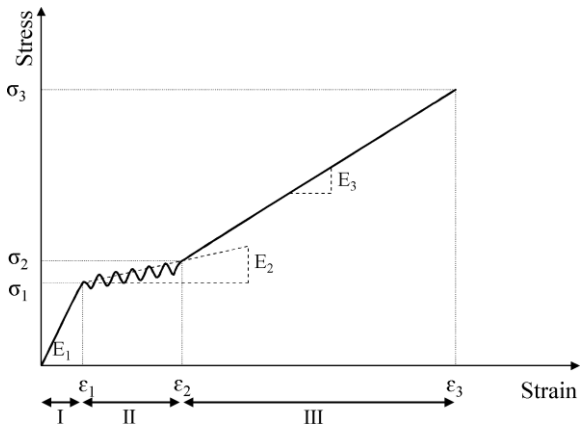

Fig. 13. Typical tensile stress-strain behavior of TRMs.

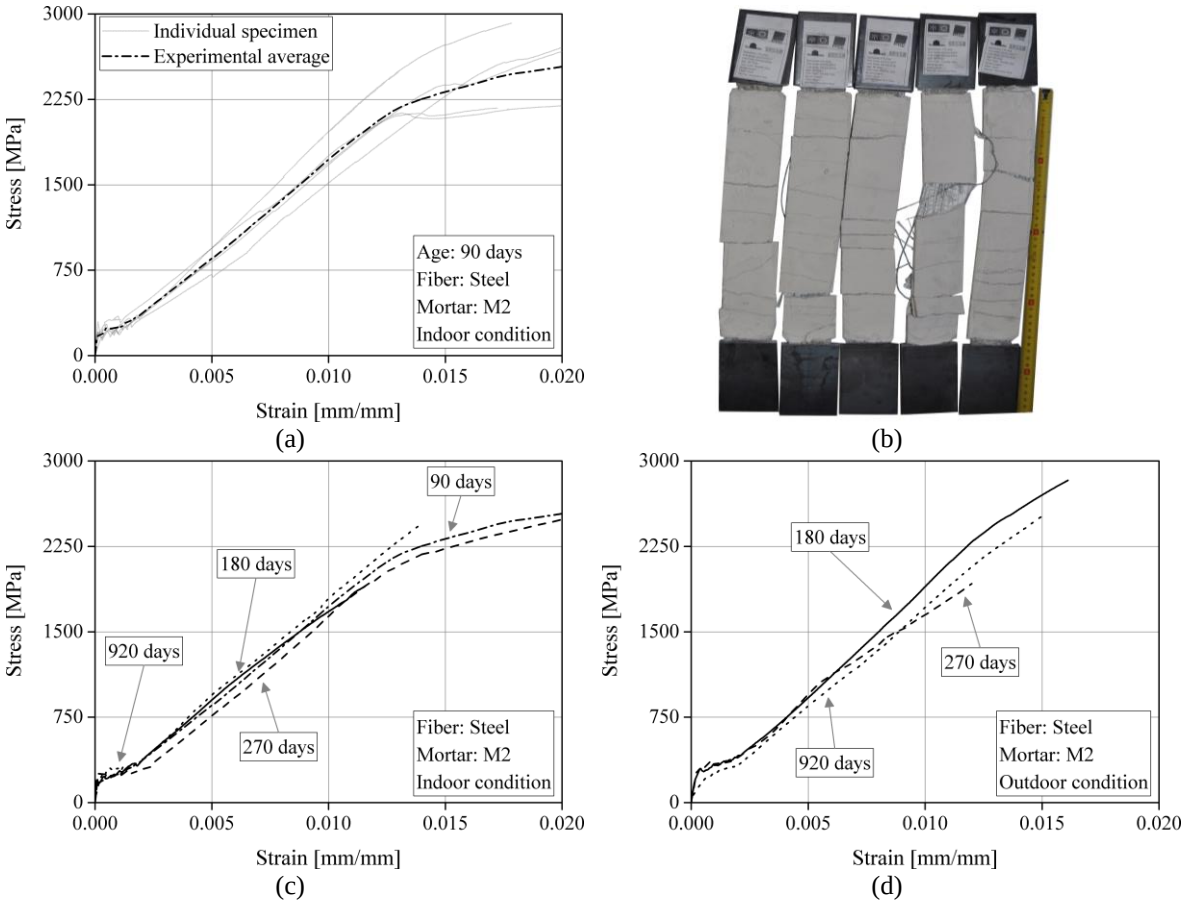

Fig. 14. Tensile response of the steel-based TRM: (a) typical tensile behavior; (b) saturated cracking stage at 90 days (indoor aged); (c) effect of the mortar age under indoor conditions; (d) effect of mortar age under outdoor conditions.

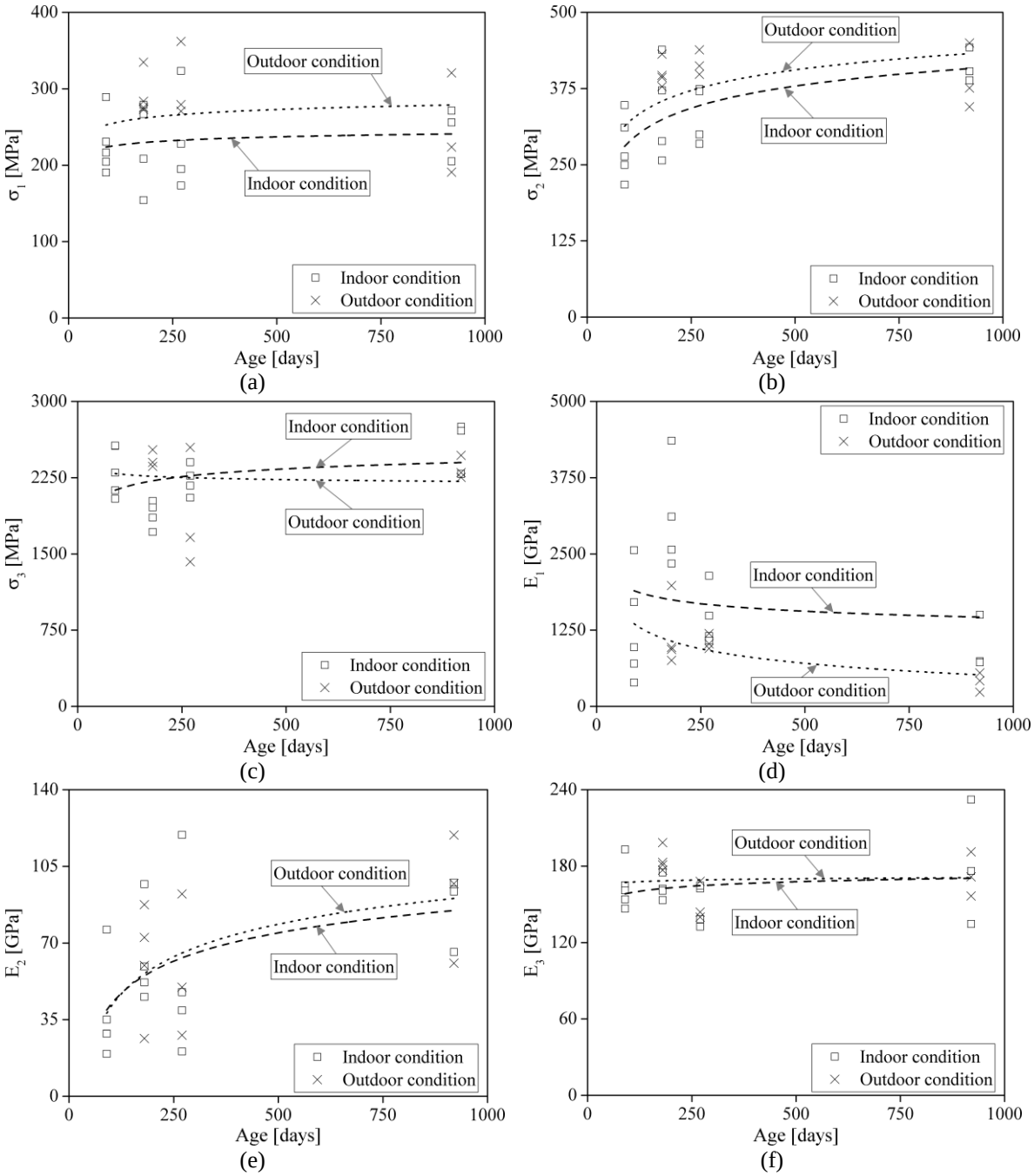

Fig. 15. Tensile response parameters of the steel-based TRM: (a) σ_1; (b) σ_2; (c) σ_3; (d) E_1; (e) E_2; (f) E_3.

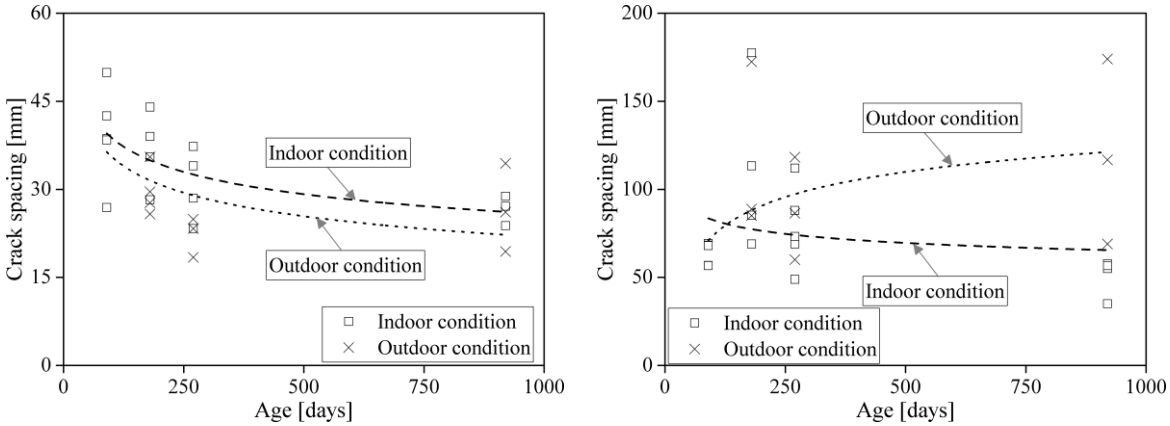

(a) (b)

Fig. 16. Crack spacing under tensile test: (a) the steel-based TRM; (b) the glass-based TRM.

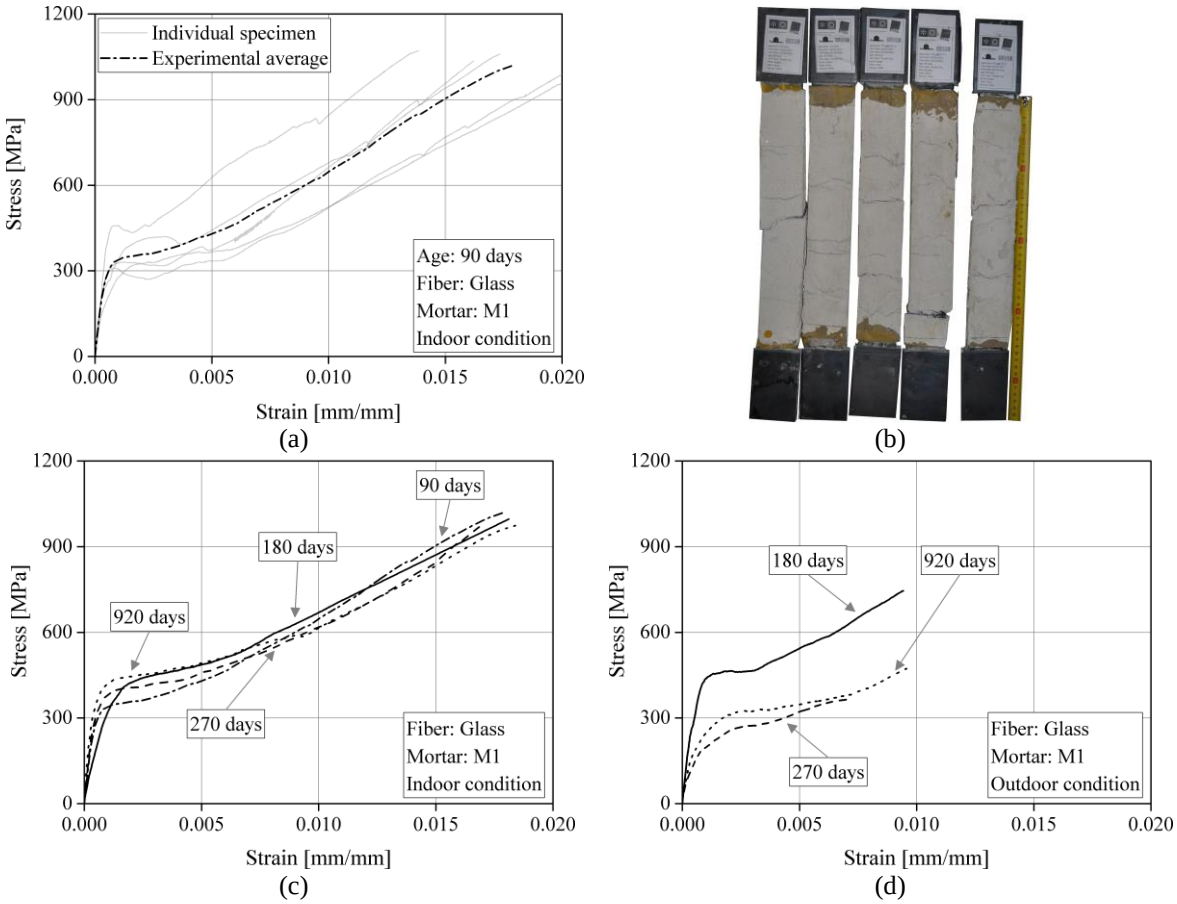

Fig. 17. Tensile response of the glass-based TRM: (a) typical tensile behavior; (b) saturated cracking stage at 90 days (indoor aged); (c) effect of the mortar age under indoor conditions; (d) effect of mortar age under outdoor conditions.

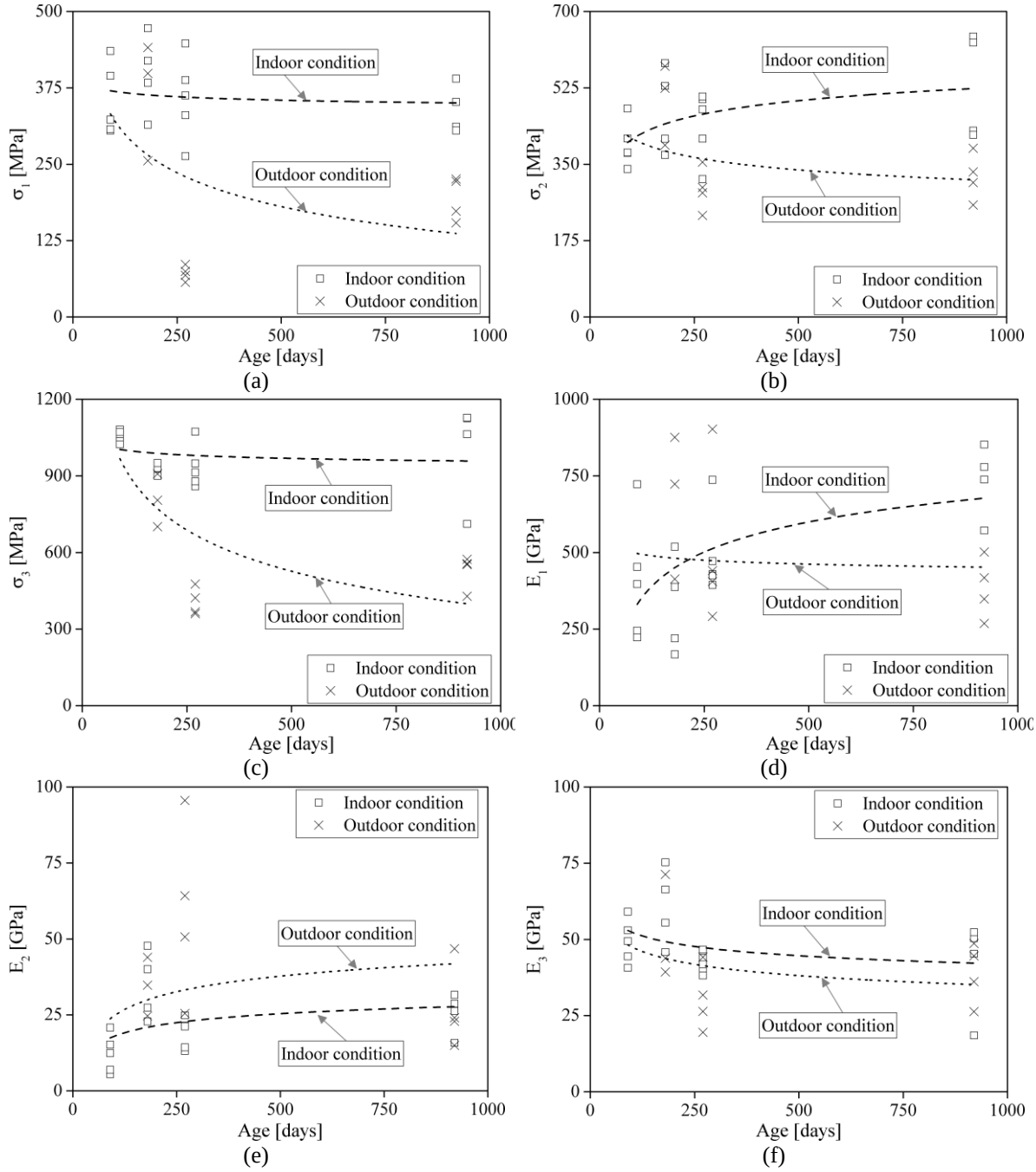

Fig. 18. Tensile response parameters of the glass-based TRM: σ_1; (b) σ_2; (c) σ_3; (d) E_1; (e) E_2; (f) E_3.

List of Tables

Table 1. Overview of the experimental tests.

Test type	Objective	Mortar	Fiber	Bond length [mm]	Age [days]
Mortar strength	effect of the mortar age on its strength	M1-M2	-	-	15
					30
					60
					90
					180
					920
	effect of the real environmental condition on the mortar strength	M1-M2	-	-	180
					920
pull-out	effect of the mortar age on the textile-to-mortar bond	M1-M2	glass-steel	50- 150	15
					30
					90
					180
					270
					920
	effect of the real environmental condition on the textile-to-mortar bond	M1-M2	glass-steel	50- 150	180
					270
					920
	effect of mortar type	M- M2	steel	150	90
					920
tensile	effect of the mortar age on the tensile behavior of TRM composites	M1-M2	glass-steel	350	90
					180
					270
					920
	effect of the real environmental condition on the tensile behavior of TRM composites	M1-M2	glass-steel	350	180
					270
					920

Table 2. Mechanical properties of mortars aged under indoor conditions.*

Mortar	Test	3 days	7 days	14 days	30 days	60 days	90 days	180 days	920 days
M1	Compressive strength (f_c) [MPa]	0.9 (4)	3.8 (5)	5.9 (8)	7.1 (9)	8.3 (11)	7.8 (4)	7.5 (10)	5.7 (12)
	f_c / $f_{c\text{-}30\ days}$ [%]	13	53	84	100	117	111	106	81
	Flexural strength (f_{ft}) [MPa]	-	2.5 (7)	4.0 (3)	4.7 (7)	5.1 (3)	5.6 (10)	6.0 (10)	5.2 (11)
	f_{ft} / $f_{ft\text{-}30\ days}$ [%]	-	53	86	100	108	109	118	102
M2	Compressive strength (f_c) [MPa]	3.9 (7)	6.5 (7)	8.8 (7)	9.5 (10)	8.8 (12)	8.9 (5)	7.5 (9)	7.9 (5)
	f_c / $f_{c\text{-}30\ days}$ [%]	41	68	92	100	92	93	79	83
	Flexural strength (f_{ft}) [MPa]	1.4 (3)	1.5 (3)	1.8 (12)	2.5 (9)	2.1 (7)	2.3 (9)	2.6 (13)	3.1 (12)
	f_{ft} / $f_{ft\text{-}30\ days}$ [%]	55	60	71	100	82	92	103	123

*Coefficients of variation in percentage terms are provided inside parentheses.

Table 3. Mechanical properties of mortars aged under outdoor conditions.*

Mortar	Test	90 days	180 days	920 days
M1	Compressive strength (f_c) [MPa]	7.8 (4)	9.7 (16)	6.6 (8)
	Flexural strength (f_{ft}) [MPa]	5.6 (10)	5.3 (7)	4.1 (11)
M2	Compressive strength (f_c) [MPa]	8.9 (5)	10.9 (12)	6.3 (5)
	Flexural strength (f_{ft}) [MPa]	2.3 (9)	2.3 (12)	2.3 (3)

*Coefficients of variation in percentage terms are provided inside parentheses.

7 APPENDIX

Table A1. Pull-out properties of the steel-based TRM aged under indoor conditions.*

Mortar	Age [days]	Slip corresponding to peak load [mm]	Peak load [N]	Debonding energy [N.mm]	Chemical bond energy [J/mm^2]	Pull-out energy [N.mm]	Initial stiffness [N/mm]	Number of specimens
M2	15	0.8 (16)	711.1 (7)	376.0 (20)	0.06 (37)	6030.6 (7)	1902.6 (19)	4
	30	0.9 (9)	871.9 (9)	529.2 (20)	0.09 (57)	8132.8 (9)	2076.1 (23)	4
	90	0.8 (3)	740.6 (9)	364.5 (10)	0.07 (16)	6763.9 (10)	1277.4 (10)	4
	180	0.9 (16)	730.9 (17)	436.8 (32)	0.04 (54)	7253.0 (16)	1360.3 (14)	4
	270	0.8 (21)	747.9 (17)	408.4 (43)	0.09 (55)	6373.3 (2)	1865 (29)	4
	920	1.02 (6)	945.3 (11)	614.8 (14)	0.06 (50)	8691.6 (8)	1889.2 (25)	3
M1	90	1.0 (12)	916.6 (8)	599 (14)	-	12514.4 (16)	2657.8 (18)	4
	920	1.1 (19)	769.2 (8)	537.0 (28)	0.01 (91)	7358.8 (13)	1202.7 (6)	4

*Coefficients of variation in percentage terms are provided inside parentheses.

Table A2. Pull-out properties of the steel-based TRM aged under outdoor conditions*.

Age [days]	Slip corresponding to peak load [mm]	Peak load [N]	Debonding energy [N.mm]	Chemical bond energy [N.mm]	Pull-out energy [N.mm]	Initial stiffness [N/mm]	Number of specimens
180	1.3 (5)	1121.5 (4)	1045.0 (11)	0.08 (35)	10139.3 (5)	2871 (27)	3
270	1.7 (6)	1550.3 (2)	1839.2 (5)	0.12 (56)	12262.0 (1)	3222.3 (13)	3
920	1.3 (36)	1125.9 (16)	971.0 (43)	0.03 (25)	9243.7 (12)	2058.5 (40)	4

*Coefficients of variation in percentage terms are provided inside parentheses.

Table A3. Bond-slip laws of the steel-based TRM aged under indoor conditions.*

Mortar	Age [days]	$\tau_{max.}$ [MPa]	τ_f [MPa]	κ [Mpa/mm]	β
M2	15	3.97 (18)	1.34 (6)	17.72 (45)	0.0001 (0)
	30	5.10 (28)	1.69 (6)	22.06 (53)	0.0004 (29)
	90	3.05 (15)	1.42 (10)	4.93 (45)	0.0003 (0)
	180	3.01 (27)	1.51 (16)	6.52 (55)	0.0005 (33)
	270	4.32 (38)	1.39 (14)	17.56 (66)	0.0003 (33)
	920	4.73 (30)	1.94 (8)	17.92 (62)	0.0006 (14)
M1	90	4.53 (20)	2.09 (14)	38.73 (35)	0.0020 (41)
	920	2.55 (13)	1.77 (10)	4.34 (30)	0.0001 (19)

*Coefficients of variation in percentage terms are provided inside parentheses.

Table A4. Bond-slip laws of the steel-based TRM aged under outdoor conditions.*

Age [days]	$\tau_{max.}$ [MPa]	τ_f [MPa]	κ [MPa/mm]	β
180	6.64 (6)	2.32 (7)	41.36 (47)	0.0005 (44)
270	10.01 (7)	3.17 (0)	45.34 (16)	0.0004 (43)
920	4.92 (28)	2.91 (11)	22.00 (100)	0.0003 (60)

*Coefficients of variation in percentage terms are provided inside parentheses.

Table A5. Pull-out properties of the glass-based TRM aged under indoor conditions.*

Age [days]	Slip corresponding to peak load [mm]	Peak load [N]	Debonding energy [N.mm]	Pull-out energy [N.mm]	Initial stiffness [N/mm]	Number of specimens
15	2.6 (12)	284.6 (10)	542.9 (16)	2279.0 (8)	456.1 (4)	4
30	1.9 (31)	250.5 (30)	380.2 (49)	2166.9 (38)	815 (22)	4
90	2.3 (13)	378.8 (16)	656.4 (8)	4554.6 (19)	857.8 (22)	4
180	2.3 (27)	390.8 (12)	648.4 (32)	5133.8 (10)	909.1 (35)	4
270	3.1 (13)	339.5 (17)	792.7 (24)	2775.7 (28)	917.3 (38)	4
920	1.9 (22)	410.9 (10)	607.6 (13)	2569.8 (28)	785.5 (43)	4

*Coefficients of variation in percentage terms are provided inside parentheses.

Table A6. Pull-out properties of the glass-based TRM aged under outdoor conditions.*

Age [days]	Slip corresponding to peak load [mm]	Peak load [N]	Debonding energy [N.mm]	Pull-out energy [N.mm]	Initial stiffness [N/mm]	Number of specimens
180	1.8 (18)	459.7 (4)	622.8 (23)	4878.2 (19)	1012.7 (18)	4
270	2.2 (11)	437.6 (15)	801.0 (21)	4461.3 (18)	1423.0 (48)	4
920	2.1 (20)	403.2 (12)	695.9 (18)	3542.4 (24)	3069.2 (2)	4

*Coefficients of variation in percentage terms are provided inside parentheses.

Table A7. Bond-slip laws of the glass-based TRM aged under indoor conditions.*

Age [days]	$\tau_{max.}$ [MPa]	τ_f [MPa]	κ [MPa/mm]	β
15	1.97 (16)	1.03 (22)	6.46 (35)	0.009 (34)
30	2.92 (28)	0.65 (34)	14.04 (49)	0.017 (51)
90	5.38 (24)	0.86 (28)	18.57 (28)	0.028 (29)
180	2.73 (24)	1.25 (11)	10.35 (69)	0.009 (76)
270	2.88 (45)	0.91 (34)	11.70 (92)	0.014 (111)
920	5.43 (37)	1.64 (12)	15.51 (63)	0.013 (58)

*Coefficients of variation in percentage terms are provided inside parentheses.

Table A8. Bond-slip laws of the glass-based TRM aged under outdoor conditions.*

Age [days]	$\tau_{max.}$ [MPa]	τ_f [MPa]	κ [MPa/mm]	β
180	6.62 (32)	1.6 (12)	26.20 (48)	0.007 (38)
270	8.94 (9)	1.37 (14)	51.17 (50)	0.013 (28)
920	8.81 (6)	0.49 (14)	101.06 (3)	0.056 (21)

*Coefficients of variation in percentage terms are provided inside parentheses.

Table A9. Tensile parameters of the steel-based TRM aged under indoor conditions.*

Age [days]	E_1 [GPa]	E_2 [GPa]	E_3 [Gpa]	ε_1 [%]	ε_2 [%]	ε_3 [%]	σ_1 [MPa]	σ_2 [MPa]	σ_3 [MPa]	Number of cracks	Distance between cracks [mm]	Number of specimens
90	1266.3 (62)	37.5 (53)	163.9 (10)	0.03 (69)	0.15 (21)	1.40 (13)	226.2 (15)	277.8 (17)	2318.4 (9)	8	39	5
180	3094.3 (25)	63.4 (31)	162.8 (5)	0.01 (17)	0.19 (8)	1.14 (8)	227.1 (22)	339.0 (21)	1887.8 (6)	9	36.7	4
270	1464.7 (29)	56.7 (66)	149.4 (10)	0.02 (19)	0.21 (19)	1.49 (10)	229.9 (25)	332.0 (12)	2223.8 (6)	11	30.8	4
920	986.8 (37)	85.6 (16)	181.0 (22)	0.03 (37)	0.22 (4)	1.51 (25)	244.1 (12)	411.4 (6)	2582.8 (8)	13	26.1	3

*Coefficients of variation in percentage terms are provided inside parentheses.

Table A10. Tensile behavior of the steel-based TRM aged under outdoor conditions. *

Age [days]	E_1 [GPa]	E_2 [GPa]	E_3 [GPa]	ε_1 [%]	ε_2 [%]	ε_3 [%]	σ_1 [MPa]	σ_2 [MPa]	σ_3 [MPa]	Number of cracks	Distance between cracks [mm]	Number of specimens
180	1159.6 (41)	61.6 (37)	184.8 (4)	0.03 (32)	0.20 (4)	1.29 (5)	291.7 (9)	399.8 (5)	2411.7 (3)	11	29.6	4
270	1057.1 (10)	56.7 (47)	150.6 (8)	0.03 (22)	0.23 (10)	1.18 (20)	303.9 (14)	416.3 (4)	1877.5 (26)	15	20	3
920	400.4 (32)	92.4 (26)	173.1 (8)	0.08 (60)	0.24 (5)	1.37 (6)	245.1 (22)	390.2 (11)	2340.9 (4)	14	25	3

*Coefficients of variation in percentage terms are provided inside parentheses.

Table A11. Tensile behavior of the glass-based TRM aged under indoor conditions.*

Age [days]	E_1 [GPa]	E_2 [GPa]	E_3 [GPa]	ε_1 [%]	ε_2 [%]	ε_3 [%]	σ_1 [MPa]	σ_2 [MPa]	σ_3 [MPa]	Number of cracks	Distance between cracks [mm]	Number of specimens
90	408.1 (44)	12.2 (46)	49.3 (13)	0.10 (40)	0.47 (25)	1.83 (18)	353.1 (15)	395.6 (12)	1054.0 (2)	4	63.8	5
180	323.3 (43)	34.5 (29)	60.7 (18)	0.14 (38)	0.46 (32)	1.68 (8)	397.4 (14)	472.6 (18)	932.5 (2)	3	102.8	4
270	491.3 (25)	19.0 (24)	42.2 (7)	0.07 (12)	0.52 (33)	1.68 (12)	358.2 (17)	440.8 (16)	934.4 (8)	4	78.2	5
920	735.3 (14)	25.6 (23)	41.6 (33)	0.05 (10)	0.77 (24)	1.98 (10)	339.6 (10)	528.8 (20)	1006.9 (17)	6	46.9	4

*Coefficients of variation in percentage terms are provided inside parentheses.

Table A12. Tensile behavior of the glass-based TRM aged under outdoor conditions.*

Age [days]	E_1 [GPa]	E_2 [GPa]	E_3 [GPa]	ε_1 [%]	ε_2 [%]	ε_3 [%]	σ_1 [MPa]	σ_2 [MPa]	σ_3 [MPa]	Number of cracks	Distance between cracks [mm]	Number of specimens
180	670.7 (29)	34.5 (23)	51.5 (27)	0.06 (13)	0.44 (18)	1.07 (18)	365.1 (22)	497.6 (15)	804.7 (10)	2	115	3
270	509.9 (46)	59.0 (43)	30.5 (30)	0.02 (42)	0.45 (33)	0.82 (24)	71.4 (15)	292.1 (15)	406.5 (11)	4	88	4
920	384.0 (22)	27.2 (44)	38.9 (22)	0.05 (32)	0.55 (21)	1.10 (21)	193.8 (16)	320.9 (15)	528.0 (11)	2	119	4

*Coefficients of variation in percentage terms are provided inside parentheses.